Sensorless Vector Control for High-Performance SPIM Drives using New Super-Twisting BS_PCH Control and VM SC MRAS Observer

PHU DIEP NGUYEN, NGOC THUY PHAM*
Faculty of Electrical Engineering Technology,
Industrial University of Ho Chi Minh City (IUH),
Nguyen Van Bao Stress, Ho Chi Minh City, Viet Nam,
VIETNAM

Abstract: - In this paper, an improved Backstepping _Port Controlled Hamiltonian (STABS_PCH) nonlinear control structure combined with a Stator Current Based Model Reference Adaptive System speed observer using neural network (VMNN_SC_MRAS) is presented. The STABS_PCH control improves and enhances the performance and robustness of SPIM drives. The combination of the STABS_PCH controller with the VMNN_SC_MRAS speed estimator can compensate for the uncertainties of the machine parameters and load disturbances to improve the dynamic performance and of robustness the SPIM sensorless drive systems. The effectiveness of the proposal control scheme is validated through Matlab-Simulink.

Key-Words: - Backstepping control, Super Twisting algorithm, FOC vector control, Six phase induction motor drive, Port Controled Hamiltonian control, Nonlinear control.

Received: May 24, 2024. Revised: October 27, 2024. Accepted: November 28, 2024. Published: December 31, 2024.

1 Introduction

Recently, Multiphase motor drives have been widely utilized in various fields due to their advantages, including higher torque density, greater efficiency, fault tolerance, and reduced torque pulsations. These features are particularly beneficial in applications such as locomotive traction, electrical ship propulsion, and high-power sectors such as automotive, aerospace, military, and nuclear industries, [1].

Now, SPIM drive systems have been widely applied in industries. To enhance the performance of the SPIM drives, various modern nonlinear control solutions have been focused on research. Among these methods, FOC Control is a method with many outstanding advantages and is widely applied in SPIM drive systems. The traditional FOC strategies using PI controllers do not meet satisfactory quality for high-performance SPIM drives, which motivates the development of nonlinear control methods to replace PID controllers [2], including the feedback linearizing control, Fuzzy Logic control (FL), neural network control (NN), slip model control (SM), Backstepping control (BS), prediction control, passive control, and Hamiltonian control, [3], [4], [5], [6], [7], [8], [9], [10], [11], [12], [13], [14], [15], [16], [17], [18].

Among these techniques, BS control has gained significant attention for its systematic and recursive design in nonlinear feedback control. Its major advantage is flexibility to avoid cancellation of useful nonlinearities while achieving stabilization and tracking goals. However, traditional BS controllers require precise knowledge of system dynamics. Various strategies have been proposed to address this limitation. In [18], a novel BS control scheme was introduced that uses a dynamical induction motor model and traditional BS control with the unknown of the damping coefficient, the motor inertia, the load torque, and the uncertainty of the machine parameters. Despite these advancements, issues such as speed ripple and poor reference speed tracking persist. In [19], [20], [21], an adaptive observer and an integral control version have been using backstepping techniques were proposed. The results show that improved control performance but increased the complexity of solving differential equations due to a greater number of model states. In [21], the BS strategy was developed for both observer and control, the integral error tracking component was added to enhance dynamic response and control precision. However, the torque ripple is recorded as quite large, and the performance at low-speed range and regenerating modes is not reported.

In this paper, to overcome above the drawbacks, an adaptive BS control is combined with a super-twisting algorithm (STABS) for the outer speed and rotor flux control loop. The STA_BS controller, besides adding the integral error tracking component

to improve its sustainability, the proposed control strategy also employs the super-twisting algorithm to enhance robustness against parameter uncertainties and external load disturbances, effectively addressing the chattering issue in traditional sliding-mode techniques. However, to enhance the performance and robustness of the FOC technique, besides the improved BS, the author also combinates the STABS method with the PCH controller for the inner current control loop to enhance the performance and stability of the drive systems. However, implementing the FOC technique requires precise speed and rotor flux (RF) information. To overcome these and to eliminate mechanical sensors for speed measurement due to their sensitivity, noise, cost, size, weight, and reduced reliability, [22]. This paper focuses on accurate rotor flux estimation and speed estimation of the improved stator current based on reference model adaptive systems (SC_MRAS) using neuron networks to improve the performance of the observer and controller for the high-performance SPIM drives. Specifically, the reference model in the proposed NN_SC_MRAS observer uses the stator current components to be free of pure integration problems and insensitive to motor parameter variations. The adaptive model uses a two-layer linear NN trained online by a linear LS algorithm. These improvements require less computation effort and overcome some drawbacks of nonlinear structure and algorithm, which was presented in literature published before, [23].

These significantly improve the performance of the proposed NN_SC_MRAS observer. Additionally, this proposed observer uses the voltage model (VM) to avoid instability in the regenerating mode, [23]. To enhance the performance of FOC strategy and observer, the stator and rotor resistance are estimated and updated for more accurate speed control and current estimation, and finally, the adaptive model employs modified Euler integration to address instability issues arising from the discretization of the rotor equations of the machine enhance the performance of observer. Integrating the STABS_PCH controller with the proposed SC_MRAS speed estimator improves stability and compensates for uncertainties from SPIM parameter variations, measurement errors, and external load disturbances. The efficacy of this proposed control and observer structure is validated through MATLAB/Simulink simulations. The paper consists of five sections: Section 2 details the SPIM drives model, Section 3 introduces the STABS_SM controller and SC_MRAS observer, and Section 4 presents the simulations and discussions. Finally, the conclusion is provided in Section 5.

2 Model of SPIM Drives

This drive system includes a Six-Phase Induction Motor (SPIM) fed by a six-phase AC Voltage Source Inverter (SPVSI). SPVSI block diagram is shown in Figure 1.

The Space Vector Analysis technique (VSD) in [18] is applied to transform the original six-dimensional space of SPIM into three orthogonal two-dimensional subspaces in the static reference frame (D-Q), (x - y), and (zl - z2). We have the transformation matrix:

$$T_6 = \frac{1}{\sqrt{3}}\begin{bmatrix} 1 & \frac{\sqrt{3}}{2} & -\frac{1}{2} & -\frac{\sqrt{3}}{2} & -\frac{1}{2} & 0 \\ 0 & \frac{1}{2} & \frac{\sqrt{3}}{2} & \frac{1}{2} & -\frac{\sqrt{3}}{2} & -1 \\ 1 & -\frac{\sqrt{3}}{2} & -\frac{1}{2} & \frac{\sqrt{3}}{2} & -\frac{1}{2} & 0 \\ 0 & \frac{1}{2} & -\frac{\sqrt{3}}{2} & \frac{1}{2} & \frac{\sqrt{3}}{2} & -1 \\ 1 & 0 & 1 & 0 & 1 & 0 \\ 0 & 1 & 0 & 1 & 0 & 1 \end{bmatrix} \quad (1)$$

The electrical matrix equations of SPIM drives in the stationary reference frame may be written as:

$$\begin{aligned} [V_s] &= [R_s][I_s] + P([L_s][I_s] + [L_m][I_r]) \\ 0 &= [R_r][I_r] + P([L_r][I_r] + [L_m][I_s]) \end{aligned} \quad (2)$$

where: [V], [I], [R], [L] and [Lm] are voltage, current, resistant, self and mutual inductance vectors, respectively. p is differential operator. Subscript r and s related to the rotor and stator resistance respectively. SPIM has the squirrel cage rotor [Vr] is zero. The (x-y), (z1-z2) subspaces only produce losses, the electromechanical conversion only was taken in the DQ subspace so the control strategies are based on determining the applied voltage in the DQ reference frame. With this transformation, the SPIM control technique is similar to the classical three-phase IM. The SPIM model transformation from (DQ) stationary reference frame into (dq) rotating reference frame to obtain currents with dc components [23] is necessary, We use a transformation matrix as follows:

$$T_{dq} = \begin{bmatrix} \cos(\delta_r) & -\sin(\delta_r) \\ \sin(\delta_r) & \cos(\delta_r) \end{bmatrix} \quad (3)$$

where δr is the rotor angular position referred to the stator.

The FOC is the most used strategy in the industrial field. In this control method, the rotor flux is controlled by *isd* stator current component and the torque by *isq* quadratic component. We have: $\psi_{rq}=0;\psi_{rd}=\psi_{rd}$. The model motor dynamics is described by the following space vector differential equations:

$$\begin{cases}\dfrac{d\omega_r}{dt}=\dfrac{3}{2}P\dfrac{\delta\sigma L_s}{J}(\psi_{rd}i_{sq})-\dfrac{T_L}{J}-B'_{\omega_r}\\ \dfrac{d\psi_{rd}}{dt}=\dfrac{L_m}{\tau_r}i_{sd}-\dfrac{1}{\tau_r}\psi_{rd}\\ L_s\dfrac{di_{sq}}{dt}=-ai_{sq}+L_s\omega_e i_{sd}+b_r\omega_e\psi_{rd}+cu_{sq}\\ L_s\dfrac{di_{sd}}{dt}=-ai_{sd}+L_s\omega_e i_{sq}+bR_r\psi_{rd}+cu_{sd}\end{cases} \quad (4)$$

where:

$$\sigma=1-\frac{L_m^2}{L_sL_r};\delta=\frac{L_m}{\sigma L_sL_r};a=\frac{L_m^2R_r+L_r^2R_s}{\sigma L_r^2};b=\frac{L_m^2R_r}{\sigma L_r^2};c=\frac{1}{\sigma};\tau_r=\frac{L_r}{R_r};B'=\frac{B}{J}$$

u_{sd},u_{sq}; i_{sd},i_{sq}: The components of stator voltage and stator current, respectively; ψ_{rd},ψ_{rq}: Rotor flux components; T_e, T_L : Electromagnetic and load torque; *d-q*; *D-Q*: Synchronous and stationary axis reference frame quantities, respectively; ω_r: the angular velocity (mechanical speed), $\omega_r = (2/P)\omega_{re}$; ω_{re}, ω_{sl}, ω_e : the electrical speed respectively Rotor and slip angular and synchronous angular velocity; L_s, L_r: Stator and rotor inductances; L_m: Mutual inductance ; R_s, R_r: Stator and rotor resistances; J: the inertia of motor and load; σ: Total linkage coefficient; P: Number of pole pairs; B: Friction coefficient; τ_r: Rotor and stator time constant.

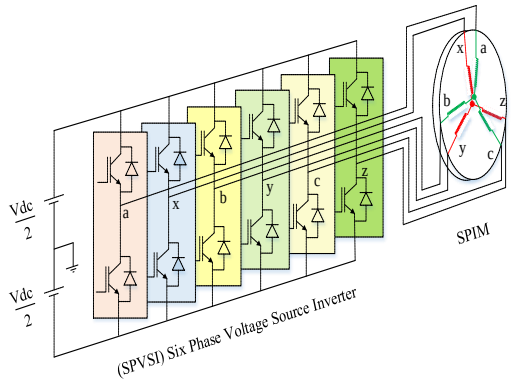

Fig. 1: A general scheme of an SPIM drive

The new expression of the electromagnetic torque and the slip frequency are given by:

$$T_e=\frac{3P}{2}\frac{L_m}{L_r}\psi_{rd}i_{sq} \quad (5)$$

$$\omega_{sl}=\frac{L_m}{L_r}\psi_{rd}i_{sq} \quad (6)$$

3 STABS_PCH Control Structure for FOC SPIM Drives

3.1 STABS Design for the Outer Speed and Flux Loops

In this part, an adaptive STA_BS control is proposed for the FOC of SPIM drives. The Lyapunov theory [2] is used in designing a control system to ensure the stability and performance. The synthesizing nonlinear control laws based on the systematic and recursive of BS technique, their equilibrium states will be ensured by a right virtual command. In the proposal, integral term of the tracking error are also is added to improved the robustness of the control system. Besides, the modified BS technique is combined with a super-twisting algorithm (STA_BS) to increase its robustness under the parameter uncertainties and external disturbances of load and eliminate the chattering problem, which exists in the traditional SM techniques.

The tracking errors of rotor flux and speed are defined:

$$\begin{aligned}\varepsilon_\omega&=\omega^*-\omega+k'_\omega\int_0^t(\omega^*-\omega)\,\mathrm{dt}\\ \varepsilon_\psi&=\psi^*_{rd}-\psi_{rd}+k'_\psi\int_0^t(\psi^*_{rd}-\psi_{rd})\,\mathrm{dt}\end{aligned} \quad (7)$$

The error dynamical equations are:

$$\begin{aligned}\dot{\varepsilon}_\omega&=\dot{\omega}^*-\frac{3}{2}n_p\frac{\delta\sigma L_s}{J}\psi_{rd}i_{sq}+\frac{T_l}{J}+B\omega+k'_\omega(\omega^*-\omega)\\ \dot{\varepsilon}_\psi&=\dot{\psi}^*_{rd}-\frac{L_m}{\tau_r}i_{sd}+\frac{1}{\tau_r}\psi_{rd}+k'_\psi(\psi^*_{rd}-\psi_{rd})\end{aligned} \quad (8)$$

The Lyapunov function is given as follow:

$$V_{(\omega,\psi)}=\frac{1}{2}(\varepsilon_\omega^2+\varepsilon_\psi^2) \quad (9)$$

Differentiating V:

$$\dot{V}_{(\omega,\psi)}=\varepsilon_\omega\dot{\varepsilon}_\omega+\varepsilon_\psi\dot{\varepsilon}_\psi=\varepsilon_\omega[\dot{\omega}^*-k_t\psi_{rd}i_{sq}+\frac{T_l}{J}+B\omega+k'_\omega(\omega^*-\omega)$$

$$+\varepsilon_{\psi_{rd}}\left\{\dot{\psi}^*_{rd}-\frac{L_m}{\tau_r}i_{sd}+\frac{1}{\tau_r}\psi_{rd}+k'_\psi(\psi^*_{rd}-\psi_{rd})\right\} \quad (10)$$

where $k_t = \frac{3}{2} n_p \frac{\delta \sigma L_s}{J}$; k_ω, k_Ψ are positive constants and are determined based on the closed-loop dynamics. The current virtual control components are chosen to V' <0 as follows:

$$i_{sq}^* = \frac{1}{k_t \psi_{rd}} \left[k_\omega \varepsilon_\omega + \frac{d\omega_r^*}{dt} + \frac{T_l}{J} + B\omega_r + k_\omega' \left(\omega_r^* - \omega_r \right) + \Pi_{\varepsilon_\omega} \right]$$
$$i_{sd}^* = \frac{\tau_r}{L_m} \left[k_\psi \varepsilon_\psi + \frac{d\psi_{rd}^*}{dt} + \frac{1}{\tau_r} \psi_{rd} + k_\psi' \left(\psi_{rd}^* - \psi_{rd} \right) + \Pi_{\varepsilon_\psi} \right] \quad (11)$$

where, $\Pi_{\varepsilon_\omega}; \Pi_{\varepsilon_\psi}$ are the control signals, which are injected to improve the Backstepping control performance. The T_L load torque is estimated as follows:

$$T_L = \frac{1}{1+\tau_0 p} \left[\left(\frac{3}{2} P \frac{L_m}{L_r} \hat{\psi}_{rd} i_{sq} \right) - \frac{J}{P} \frac{d\omega}{dt} \right]; \quad (12)$$

where τ_0: is time gain; p: differential.

With the Super-Twisting algorithm used, a control law is established as follows:

$$u = -\lambda |S|^\rho \, sat(S) + u_1 \quad (13)$$

$$\text{with:} \quad \frac{d}{dt} u_1 = \begin{cases} -u & |u| > U_M \\ -\xi \, sat(S) & |u| \le U_M \end{cases} \quad (14)$$

where: $\lambda; \xi; U_M$ là are positive design constants and $0 < \rho \le 0.5$

From Eq. (14), these signals are defined as:

$$\begin{cases} \Pi_{\varepsilon_\omega} = -\lambda_\omega |\varepsilon_\omega|^{0.5} \, sat(\varepsilon_\omega) - \xi_\omega \int sat(\varepsilon_\omega) dt \\ \Pi_{\varepsilon_\psi} = -\lambda_\psi |\varepsilon_\psi|^{0.5} \, sat(\varepsilon_\psi) - \xi_\psi \int sat(\varepsilon_\psi) dt \end{cases} \quad (15)$$

where, $\lambda_\omega; \lambda_\psi; \xi_\omega; \xi_\psi$ are positive constants.

From Eq. (11- 12) and Eq. (15), we get:

$$\frac{dV_{(\omega,\psi)}}{dt} = -k_\omega \varepsilon_\omega^2 - k_\psi \varepsilon_\psi^2 - \varepsilon_\omega \Pi_{\varepsilon_\omega} - \varepsilon_\psi \Pi_{\varepsilon_\psi} < 0 \quad (16)$$

The selection of the current virtual control components for outer loop in Eq. (11) meets the control objectives and these components also reference input which is provided to the inner loop when designing the PCH controller. The STABS control block diagram is shown in Figure 2.

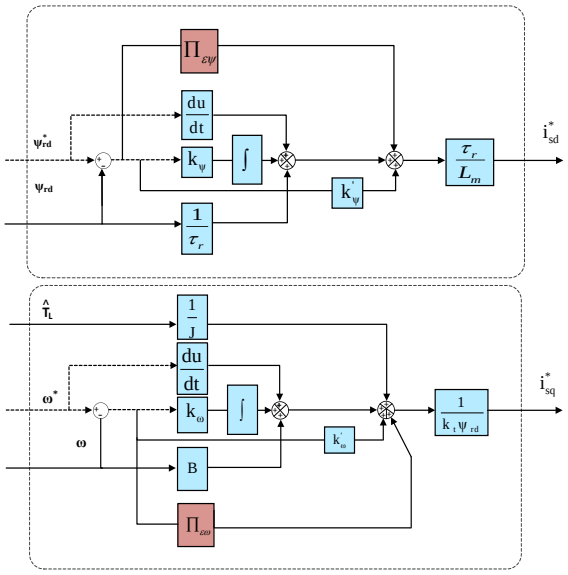

Fig. 2: *isd*, isq** Virtual vector of outer speed and RF control loop

3.2 PCH Control based on the Inner Current -Loop Controllers

The PCH system has dissipation represented as follows:

$$\begin{cases} \frac{dx}{dt} = \left[J(x) - R(x) \right] \frac{dH}{dx}(x) + g(x) u \\ y = g^T(x) \frac{dH}{dx}(x) \end{cases} \quad (17)$$

We define the state vector, the input and output vector, respectively:

$$\begin{cases} x = \begin{bmatrix} x_1 & x_2 \end{bmatrix}^T = \begin{bmatrix} L_s i_{sd} & L_s i_{sq} \end{bmatrix}^T \\ u = \begin{bmatrix} u_1 & u_2 \end{bmatrix}^T \; with: u_1 = bR_r \psi_{rd} + cu_{sd}; u_2 = -b\omega_r \psi_{rd} + cu_{sq} \\ y = \begin{bmatrix} i_{sd} & i_{sq} \end{bmatrix}^T \end{cases}$$

The interconnection structure is captured in matrix $g(x)$ and the skew symmetric matrix $J_x = -J_x^T$, $R_x = R_x^T > 0$ represents the dissipation, $H(x)$ is the total stored energy function of the system.

The Hamiltonian function of the system is given by

$$H(x) = \frac{1}{2} x^T D^{-1} x = \frac{1}{2} \left(x_1^2 + x_2^2 \right) = \frac{1}{2} \left(L_s i_{sd}^2 + L_s i_{sq}^2 \right); where, D = diag \{ L_s \quad L_s \} \quad (18)$$

SPIM equation described in a *(dq)* reference frame Eq. (5) was rewritten in the PCH form Eq. (17) with:

$$\begin{cases} J(x)=\begin{bmatrix} 0 & L_s\omega_s \\ -L_s\omega_s & 0 \end{bmatrix} \\ R(x)=\begin{bmatrix} a & 0 \\ 0 & a \end{bmatrix}; \quad g(x)=\begin{bmatrix} 1 & 0 \\ 0 & 1 \end{bmatrix} \end{cases} \tag{19}$$

Suppose that we want to the SPIM drive system to be asymptotically stabilize around a (xo) desired equilibrium, a closed-loop energy function Hd (x) is assigned to the system which has a strict minimum at x0 (that is, Hd (x) > Hd (x0) for all x . x0 in a neighborhood of x0 [17]. Given J(x), R(x), H(x) , g(x) and the desired equilibrium xo. Assume we can find a feedback control u = α(x), Ra(x), Ja(x) and a vector function K(x) satisfying:

$$\left[J_d(x)-R_d(x)\right]K(x)=-\left[J_a(x)-R_a(x)\right]\frac{dH}{dx}(x)+g(x)u \tag{20}$$

and such that

$$\begin{aligned} &\frac{dK}{dx}(x)=\left[\frac{dK}{dx}(x)\right]^T; \\ &K(x_0)=-\frac{dH}{dx}(x_0); \\ &\frac{dK}{dx}(x_0)>\frac{d^2H}{d^2x}(x_0); \end{aligned} \tag{21}$$

The closed-loop system:

$$\frac{dx}{dt}=\left[J_d(x)-R_d(x)\right]\frac{dH_d}{dx}(x) \tag{22}$$

will be a PCH system with dissipation.

$$K(x)=\frac{dH_a}{dx}; H_a(x)=H_d(x)-H(x) \tag{23}$$

where H_a is the energy added to the system and x_0 will be a stable equilibrium of the closed-loop system. The expected Hamiltonian energy storage function is defined as:

$$H_d(x)=H(x) \quad with: \quad x=x-x_0 \tag{24}$$

where

$$\begin{aligned} &J_d(x)=J(x)+J_a(x)=-J_d^T(x); \\ &R_d(x)=R(x)+R_a(x)=R_d^T(x)>0; \\ &J_a(x)=\begin{bmatrix} 0 & J_1 \\ -J_1 & 0 \end{bmatrix}; R_a(x)=\begin{bmatrix} r_1 & 0 \\ 0 & r_2 \end{bmatrix} \end{aligned} \tag{25}$$

where, r1 and r2, J1 are undetermined interconnect and damping, respectively. The voltage virtual vector components are chosen based on Eq.(20 - 5) for the inner current loop controller are

$$\begin{cases} u_{sd}=\sigma\left[ai_{sd}^*+r_1\left(i_{sd}^*-i_{sd}\right)-J_1\left(i_{sq}^*-i_{sq}\right)-L_s\omega_s i_{sq}^*-bR_r\psi_{rd}\right] \\ u_{sq}=\sigma\left[ai_{sq}^*+r_2\left(i_{sq}^*-i_{sq}\right)+J_1\left(i_{sd}^*-i_{sd}\right)+L_s\omega_s i_{sd}^*+b\omega_r\psi_{rd}\right] \end{cases} \tag{26}$$

We see that the ψ_{rd} RF component in Eq. (11) and Eq. (6) cannot measured so this paper proposes to identify this rotor flux component by VM and this is presented in part 3.3.3.

3.3 VMNN_SC_ MRAS Speed Observer

3.3.1 Structure of the VMNN_SC_ MRAS Speed Observer

The NNSC_MRAS speed observer includes a reference model, an adaptive model, and an adaptation mechanism to estimate speed, with a structural diagram as shown in Figure 5 (Appendix). In this proposed observer, the measured stator current components of the SPIM are used as a reference model.

The adaptive model is computed by combining the current and voltage models (VM and CM) [17] and is and is represented as follows:

$$\dot{x}=Ax+Bu \tag{27}$$

where

$$x=\begin{bmatrix} i_{sD} \\ i_{sQ} \end{bmatrix}; A_x=\begin{bmatrix} -\left(R_s+\frac{L_m^2}{L_r^2T_r}\right)\frac{1}{\sigma L_s} & \\ & -\left(R_s+\frac{L_m^2}{L_r^2T_r}\right)\frac{1}{\sigma L_s} \end{bmatrix}; B_x=\begin{bmatrix} \frac{1}{\sigma L_s} & 0 & \frac{1}{\sigma L_s}\frac{L_m}{L_rT_r} & \frac{1}{\sigma L_s}\frac{\omega_r L_m}{L_r} \\ 0 & \frac{1}{\sigma L_s} & -\frac{1}{\sigma L_s}\frac{\omega_r L_m}{L_r} & \frac{1}{\sigma L_s}\frac{L_m}{L_rT_r} \end{bmatrix}; u_s=\begin{bmatrix} u_{sD} \\ u_{sQ} \\ \psi_{rD} \\ \psi_{rQ} \end{bmatrix} \tag{28}$$

Therefore, the corresponding discrete model of the system is given:

$$\hat{X}(k)=e^{A_xT_s}X(k\text{-}1)+\left[e^{A_xT_s}-I\right]A_x^{-1}B_x u_s(k\text{-}1) \tag{29}$$

$e^{A\,T_s}$: is usually calculated by truncating its power series expansion, i.e.,

$$e^{A_xT_s}=I+\frac{A_xT_s}{1!}+\frac{A_x^2T_s}{2!}+....+\frac{A_x^nT_s}{n!} \tag{30}$$

If n=1, the simple forward Euler method is obtained, which gives the following finite difference equation, [24].

$$\begin{aligned} &\hat{i}_{sD}(k)=w_1\hat{i}_{sD}(k-1)+w_2u_{sD}(k-1)+w_3\hat{\psi}_{rd}(k-1)+w_4\hat{\psi}_{rq}(k-1) \\ &\hat{i}_{sQ}(k)=w_1\hat{i}_{sQ}(k-1)+w_2u_{sQ}(k-1)+w_3\hat{\psi}_{rq}(k-1)-w_4\hat{\psi}_{rd}(k-1) \end{aligned} \tag{31}$$

where marks the variables estimated with the adaptive model and is the current time sample. The neural network weights in Eq. (31) are defined as:

$$w_1=1-\frac{T_sR_s}{\sigma L_s}-\frac{T_sL_m^2}{\sigma L_sL_rT_r}; \; w_2=\frac{T_s}{\sigma L_s}; \; w_3=\frac{T_sL_m}{\sigma L_sT_r}; w_4=\frac{T_sL_m}{\sigma L_sL_r}\hat{\omega}_r \tag{32}$$

where: $\hat{i}_s(k)$ the current components are estimated by the adaptive model, k,Ts: the current and the

stator current observer time sample, respectively. Neural networks have four inputs and two outputs, in that, the w1, w2, and w3 weights are kept constant and equal to their offline computed values, w4 weight is adopted online, [17].

In this proposed VMNN_SC_MRAS speed observer improved the adaptive model by using the ADALINE, and replacing the nonlinear used in the BPN by a suitable linear least-square algorithm to overcome some drawbacks due to the nonlinearity and reduce the computation effort for the system.

Furthermore, using the adaptive model in prediction mode enhances algorithm convergence speed, improves speed control loop bandwidth, optimizes zero-speed performance, and reduces estimation errors in both transient and steady states. An more effective integration method than that used in Eq. (29) is called the modified Euler integration, this method also considers the values of the variables in two previous time steps, [17]. The neural networks reproduced these equations, with the neural network weights defined as Eq. (33).

$$\begin{aligned} i_{sD}(k) &= w_1 i_{sD}(k-1) + w_2 u_{sD}(k-1) + w_3 \psi_{rd}(k-1) + w_4 \psi_{rq}(k-1) + w_5 i_{sD}(k-2) - w_6 u_{sD}(k-2) \\ i_{sQ}(k) &= w_1 i_{sQ}(k-1) + w_2 u_{sQ}(k-1) + w_3 \psi_{rq}(k-1) - w_4 \psi_{rd}(k-1) + w_5 i_{sQ}(k-2) - w_6 u_{sQ}(k-2) \\ &- w_7 \psi_{rD}(k-2) - w_8 \psi_{rQ}(k-2) \\ &- w_7 \psi_{rQ}(k-2) + w_8 \psi_{rD}(k-2) \end{aligned} \tag{33}$$

$$w_1 = 1 - \frac{3TR_r}{2\sigma L_s} - \frac{3TL_m^2}{2\sigma L_s L_r T_r};\ w_2 = \frac{3T}{2\sigma L_s};\ w_3 = \frac{3TL_m}{2\sigma L_s L_r T_r};\ w_4 = \frac{3TL_m}{2\sigma L_s L_r}\omega_r;\ w_5 = \frac{3TR_r}{2\sigma L_s} + \frac{TL_m^2}{2\sigma L_s L_r T_r};$$
$$w_6 = \frac{T}{2\sigma L_s};\ w_7 = \frac{TL_m}{2\sigma L_s L_r T_r};\ w_8 = \frac{TL_m}{2\sigma L_s L_r}\omega_r \tag{34}$$

After rearranging Eq. (33) we get the equation of the matrix in prediction mode and these equations can be solved easily by any LS technique. Eq. (33) is written as: Ax $\approx$ b, It is easy to see that it is a classical matrix equation type, where A is called a "data matrix", x is the scalar unknown variable and b is the "observation vector". In this proposal, a classical LS technique in a recursive form was used, it is presented in [17]. There are three LS techniques that are the Ordinary Least-Squares (OLS) technique, the Total Least-Squares (TLS) technique, and the Data Least-Squares(DLS) technique. The LS_SC_ MRAS speed observer block diagram is shown in Figure 3.

In this paper, the authors used the OLS technique. We have:

$$A\,\hat{\omega}_r(k-1) = b \tag{35}$$

where

$$A = \begin{bmatrix} \frac{3T_s L_m}{2\sigma L_r L_s}\hat{\psi}_{rq}(k-1) - \frac{T_s L_m}{2\sigma L_r L_s}\hat{\psi}_{rq}(k-2) \\ -\frac{3T_s L_m}{2\sigma L_r L_s}\hat{\psi}_{rd}(k-1) + \frac{T_s L_m}{2\sigma L_r L_s}\hat{\psi}_{rd}(k-2) \end{bmatrix}$$

$$b = [W][Y]$$

$$[W] = \begin{bmatrix} 1 & -w_1 & -w_3 & -w_5 & w_7 & -w_2 & w_6 \end{bmatrix}^T$$

$$[Y] = \begin{bmatrix} X & U_s \end{bmatrix}$$

$$[X] = \begin{bmatrix} \hat{i}_{s\alpha}(k) & i_{s\alpha}(k-1) & \hat{\psi}_{rd}(k-1) & i_{s\alpha}(k-2) & \hat{\psi}_{rd}(k-2) \\ \hat{i}_{s\beta}(k) & i_{s\beta}(k-1) & \hat{\psi}_{rq}(k-1) & i_{s\beta}(k-2) & \hat{\psi}_{rq}(k-2) \end{bmatrix}$$

$$[U_s] = \begin{bmatrix} u_{s\alpha}(k-1) & u_{s\alpha}(k-2) \\ u_{s\beta}(k-1) & u_{s\beta}(k-2) \end{bmatrix}$$

Ax ~ b is the linear regression problem. By using a parameterized formulation (generalized LS) of the function error it is easy to generalize all problems of LS. This error is defined:

$$E_{LS} = \frac{(Ax-b)^T(Ax-b)}{1-\xi+\xi X^T X} \tag{36}$$

where T represents the transpose and ξ is equal to 0.5 for TLS, 1 for DLS and 0 for OLS.

In this paper, the OLS algorithm is used so this error is give as:

$$E_{OLS} = (Ax-b)^T(Ax-b) \tag{37}$$

where:

$$(Ax-b) = \varepsilon = \begin{bmatrix} \varepsilon_{isD} \\ \varepsilon_{isQ} \end{bmatrix} = \begin{bmatrix} i_{sD}(k) - \hat{i}_{sD}(k) \\ i_{sQ}(k) - \hat{i}_{sQ}(k) \end{bmatrix} \tag{38}$$

This error can be minimized with a gradient descent method:

$$\omega_r(k+1) = \omega_r(k) - \eta\gamma(k)\,a(k) \tag{39}$$

where

$$\gamma(k) = a(k)^T a(k) - b(k) \tag{40}$$

where η is the learning rate, a(k) is the row of A fed at instant k, and b(k) is the corresponding observation.

3.3.2 Rotor Speed Estimation Algorithm:

3.3.2.1 RF and Online Rs Rr estimator

From Eq. (30), we can be seen that with the information on the rotor speed, stator voltages and rotor flux, the adaptive model will generate the

stator current values. The rotor flux in Eq. (30) was estimated based on VM as follows:

$$\frac{d\hat{\psi}_{rd}}{dt} = \frac{L_r}{L_m}(u_{sD} - R_s i_{sD} - \sigma L_s \frac{di_{sD}}{dt});$$
$$\frac{d\hat{\psi}_{rq}}{dt} = \frac{L_r}{L_m}(u_{sQ} - R_s i_{sQ} - \sigma L_s \frac{di_{sQ}}{dt}); \quad (41)$$

Eq. (41) shows that from the measured stator current and voltage we can estimate the rotor flux components. Employing the Voltage Model as in Eq. (41) will help overcome the problem of instability in the regenerating mode operation.

When estimating the rotor speed Eq. (38) shows that the parameters of the rotor and stator resistance are required. However, during the operation of the machine, the resistance parameters Rs and Rr will change as the temperature increases, especially, during low-speed operation. Therefore, to improve the performance of the observer, online Rs and Rr resistance estimation are necessary.

In particular, Rs is estimated on the basis of the i_{sD}, i_{sD} measured and $\hat{i}_{sD}, \hat{i}_{sQ}$ estimated stator current components , by means of the following update law:

$$\frac{d\hat{R}_s}{dt} = -\mu((i_{sD} - \hat{i}_{sD})\hat{i}_{sD} + (i_{sQ} - \hat{i}_{sQ})\hat{i}_{sQ}) \quad (42)$$

where μ is a positive constant.

Rr Rotor resistance is estimated based on its proportional variation to Rs stator resistance as the basis of the following law:

$$\hat{R}_r = K_r \hat{R}_s \quad (43)$$

where *Kr* is the ratio of the stator and rotor resistances rated values. The estimated stator and rotor resistance values were update to the stator current observer to improve the performance the observer.

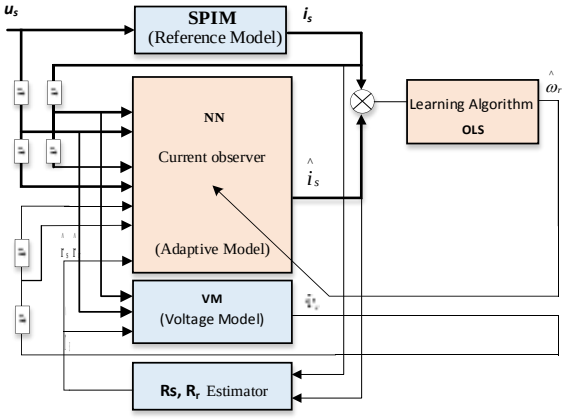

Fig. 3: OLS_ SC_ MRAS speed observer

4 Simulink and Discussion

To verify the performance of novel sensorless control strategy for SPIM drives that combine STABS_PCH new nonlinear control with VMNN_SC_MRAS rotor speed observer, many surveys have been conducted with the different motor speed and load disturbance operation mode through Matlab-Simulink. Tests have been carried out based on recommended benchmark tests in [6], [10], [11], [15], [17]. An overview diagram of the proposed sensorless strategy is shown in Figure 4 (Appendix).

SPIM parameters: 220V, 50 Hz, 4 pole, 1450 rpm. Rs = 10.1Ω, Rr = 9.8546Ω, Ls = 0.833457 H, Lr = 0.830811 H, m = 0.783106H, Ji = 0.0088 kg.m2. Rs is nominal value of stator resistance.

In this test, the proposed strategy is compared with the feedback linearizing control FLC in [10] and sliding mode controller that was proposed in [11]. Figure 5 (Appendix) shows the motor speed, isq torque current, torque, and rotor flux RF responses. The reference rotor speed is a reversal from 100 rad/s to - 100rad/s, and then this speed is set up to be surveyed at very low-speed regions (10rad/s) during 2s-3s. The load torque is provided at time t=1s with rated value and then is rejected at time t = 2.5s.

Another survey was conducted with the reference speed is reversed from 150 rad/s to -150 rad/s at time t=1s, andapplied in 100% rated load disturbance at 0.5s with the proposed controller and controller in [17] to establish a comparison framework is also also conducted.

The obtained simulation results in Figure 6 (Appendix) show that SPIM gives dynamic responses for the proposed controllers have been very well, and the speed overshoot, isD, isQ stator current components, torque, and rotor flux RF in transient operation modes do not appear. However, observing these responses is easy to see the STABS_PCH control makes fast dynamic, and stable responses more than the proposed controllers in [10], [11], [15], [17], tracking error and estimate error of almost zero and do not appear the small oscillations as the feedback linearizing controller scheme in Figure 6 of [10] the torque and rotor flux responses do not appear the overshoot and oscillation that were shown in Figure 6, Figure 7 and Figure 9 of [11]. The convergence time and transient time with a reference value of controllers in [10], [11], [15], [17] are slower, and tracking errors increase higher when applying load torque than STABS_PCH controller.

With the proposed STABS_PCH sensorless control scheme in this paper, the rotor speed

tracking the reference rotor speed is very good even having the sudden change of load torque, the convergence time of the speed with reference value is fast, the isq torque current and torque respond almost instantly. The torque and rotor flux is also more effectively controlled. The overshoot and oscillation of the torque and rotor flux responses have not been recorded. The isq torque current and torque respond almost instantly. The rotor flux has been controlled very well and been kept constant during the survey process.

From the above analysis, it is shown that the dynamic performance of the STABS_PCH control strategy for FOC vector control works very well when used in conjunction with the proposed VMNN_MRAS observer under various operating conditions, such as, it exhibits strong performance to abrupt step changes in reference speed command, as well as in handling external load disturbances, this observer and controller setup maintains its efficiency and effectiveness even when operating in the challenging low-speed region.

Another test is implemented according to Benchmark tests recommended in [6] to confirm the robustness, stability and performance of the proposed STABS_PCH control and speed observer when operating at low-speed range under the load disturbance and regenerating modes. The reference speed setup at the initial time from 0 to 0.5 seconds is zero, after increasing to 10 rad/s and is kept constant at this value and is set to reverse from 10 rad/s to - 10 rad/s at 1.5 s and kept constant until 3.5 s reversed from - 10 rad/s to 2 rad/s and kept at this value until 5.8 s and so on continuously set to reverse from 2 rad/s to - 5 rad/s at 8s, kept constant until 9.25 s, then reduced to 0, and increased again to 5 rad/s at 10s. Specifically: setup time: [0 1.5 3.5 5.8 8 9.25 10 12], reference speed value respectively: [0 10 -10 2 -5 0 5 5].

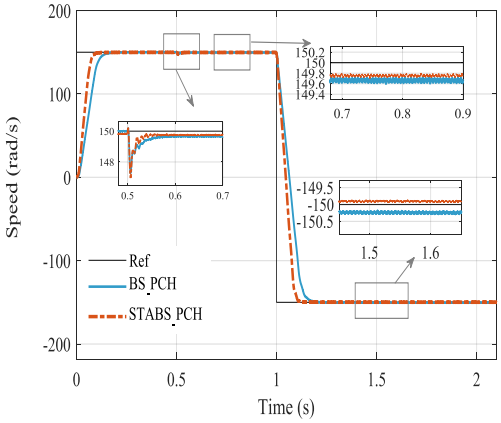

Fig. 6: Compare the speed response of BS_PCH and STA BS_PCH

The obtained results in Figure 7 show the speed estimation and reference speed tracking errors are zero even in the zone of unobservability for the interval of [0-1,5s], the speed crosses the zero-speed region very well. SPIM works robust and exactly regenerating modes and load disturbance.

The speed, rotor flux, stator current, torque in the low-speed case, and regenerating modes are controlled very well.

Comparing the survey results of the sliding mode controller using the FM-MRAS observer controller in [6] shows that the proposed controller provided faster and more accurate responses of the speed, torque, rotor flux, and stator current. In the low-speed region, when load disturbances appear the speed is almost unaffected still tracking very well the reference speed, however, comparing with the control and observation strategy that is proposed in this paper, we see that the STABS_PCH controller gets the more accurate speed response, the STABS_PCH controls isq and isd current components are quite well, the torque, current, and flux responses do not appear to oscillation phenomenon, observing Figure 9 and Figure 10 of [6] ripple torque is reported to be quite large.

5 Conclusion

This paper has proposed a new STABS_PCH control scheme combined with an adaptive VMNN_SCMRAS speed observer for sensorless FOC of SPIM drives. The STABS technique using the integral tracking errors action and well-known super-twisting algorithm to increase its robustness under uncertainties and external load disturbances is developed in the design of the rotor flux and speed controllers. PCH controller is proposed for the inner current control loop, the stabilization of the controller is achieved via system passivity. The difference between the physical energy of the system and the energy supplied by the controller is equal he closed-loop energy function. On the other hand, in order to guarantee the good performances for the SPIM drives without the use of speed sensor, the FOC vector control combined VMNN_SCMRAS speed observer. The obtained results demonstrated the effectiveness of the proposed control and observer.

References:

[1] E. Levi, Multiphase electric machines for variable-speed applications, *IEEE Transactions on Industrial Electronics*, Vol. 55, No.5, 2008, pp.1893-1909.

[2] J. W. Finch and D. Giaouris, "Controlled AC electrical drives," *IEEE Trans. Ind. Electron.*, Vol. 55, No.2, 2008, pp. 481-491.

[3] T. Taniguchi, M. Sugeno, "Piecewise Nonlinear Modeling Approach to Design Nonlinear Controllers Using Input-Output Feedback Linearization for Discrete-Time Nonlinear Systems," *25th International Conference on System Theory, Control and Computing (ICSTCC)*, Romania, , 2021, pp. 52-57.

[4] A. Accetta, M. Cirrincione, F. D'Ippolito, M. Pucci and A. Sferlazza, "Input-Output Feedback Linearization Control of a Linear Induction Motor Taking into Consideration its Dynamic End-effects and Iron Losses," *2020 IEEE Energy Conversion Congress and Exposition (ECCE)*, Detroit, MI, USA, 2020, pp. 2419-2424.

[5] Y. Kali, J. Rodas, J. Doval-Gandoy, M. Ayala, O. Gonzalez, "Enhanced Reaching-Law-Based Discrete-Time Terminal Sliding Mode Current Control of a Six-Phase Induction Motor," *Machines*, vol. 11, no. 1, p. 107, 2023.

[6] M. Touam, M. Chenafa, S. Chekroun, R. Salim, Sensorless nonlinear sliding mode control of the induction machine at very low speed using FM-MRAS observer, *International Journal of Power Electronics and Drive Systems*, Vol.12, No.4. 2021, pp. 1987-1998.

[7] N.T. Pham, D.T. Le, A Novel FOC Vector Control Structure Using RBF Tuning PI and SM for SPIM Drives, *International Journal of Robotics and Control Systems*, vol. 13, no. 5, 2020, pp. 429-440.

[8] Zellouma, D., Benbouhenni, H., Bekakra, Y. "Backstepping Control Based on a Third-order Sliding Mode Controller to Regulate the Torque and Flux of Asynchronous Motor Drive", *PP Electrical Engineering and Computer Science*, vol. 67, no.1, 2023, pp. 10-20.

[9] M.R Jovanovic, B. Bamieh, "Architecture Induced by Distributed Backstepping Design", *IEEE Transactions on Automatic Control*, Vol. 52, No.1, 2007, pp. 108-113.

[10] A. Sabir, S. Ibrir, "Induction motor speed control using reducedorder model", *AUTOMATIKA*, Vol.59, N0.3, 2018, pp. 275-286.

[11] Abdelkader Ghezouani, Brahim Gasbaoui, and Jamel Ghouili, "Sliding Mode Observer-based MRAS for Sliding Mode DTC of Induction Motor: Electric Vehicle ", *International Journal on Electrical Engineering and Informatics*, Vol. 11, No.3, 2019, pp. 580-595.

[12] Yassine Zahraoui, Mohamed Akherraz, Alfian Ma, A Comparative Study of Nonlinear Control Schemes for Induction Motor Operation Improvement, *International Journal of Robotics and Control Systems*, Vol. 2, No. 1, 2022, pp. 1-17.

[13] Abougarair, A., Aburakhis, M., & Edardar, Adaptive Neural Networks Based Robust Output Feedback Controllers for Nonlinear Systems, *International Journal of Robotics and Control Systems*, vo. 3, no.1, 2022, pp. 37-56.

[14] M. S. Mubarok, N. V. Laksmi B, Predictive controllers for synchronous reluctance motor drive systems, *International Journal of Power Electronics and Drive Systems*, Vol. 15, No. 1, 2024, pp. 98-108.

[15] Ngoc Thuy Pham, Discrete-time Sensorless Control Using new BS_SM Controller structure and VM_ SC MRAS Adaptive Speed Observer for The propulsion system of Ship, *WSEAS Transactions on Systems and Control*, Vol 19, 2020, pp.257-267, https://doi.org/10.37394/23201.2020.19.28.

[16] K. Baazouzi, S. Drid and L. Chrifi-Alaoui, "Improving the Scalar Control of Induction Motor Using Passivity Based Control," *2024 2nd International Conference on Electrical Engineering and Automatic Control (ICEEAC)*, Setif, Algeria, 2024, pp. 1-6.

[17] Ngoc Thuy Pham, Khuong Huu Nguyen, "Novel Nonlinear Control Structure for Vector Control of SPIM Drive using BS_PCH ".*International Journal of Power Electronics and Drive Systems* , Vol.11, no.3, 2020.

[18] Hou-Tsan Lee, Fu Li-Chen, Lian Feng-Li. Sensorless adaptive backstepping speed control of induction motor. In: *Proceedings of the 45th IEEE conference on decision and control*. USA;, 13–15 December 2006. pp. 1252–1257.

[19] Mehazzem F, Nemmour AL, Reama A, Benalla H. Nonlinear integral backstepping control for induction motors. *In: Proceedings of 2011 international Aegean conference on electrical machines and power electronics and Electromotion Joint Conference (ACEMP)*, Istanbul, Turkey, 2011, p. 331–36 DOI: 10.1109/ACEMP.2011.6490619.

[20] Traoré D, De Leon J, Glumineau A. Sensorless induction motor adaptive observer-

backstepping controller: experimental robustness tests on low frequencies benchmark. *IET Control Theory Appl*, Vol. 48, no.10, 2010, pp.1989-2002.

[21] Abderrahmen Zaafouri, Chiheb Ben Regaya , Hechmi Ben Azza, Abdelkader Châari, zDSP-based adaptive backstepping using the tracking errors for high-performance sensorless speed control of induction motor drive, *ISA Transactions*, Vol. 60, 2016, pp. 333-347.

[22] Holtz, "Sensorless control of induction motor drives," *Proc. of the IEEE,* Vol. 90, no.8, 2002, pp. 1359-1394.

[23] Shady M. Gadoue, Damian Giaouris, and John W. Finch , "Stator current model reference adaptive systems speed estimator for regenerating-mode low-speed operation of sensorless induction motor drives*," IET Electr. Power Appl*., Vol. 7, No.7, 2013, pp. 597-606.

Contribution of Individual Authors to the Creation of a Scientific Article (Ghostwriting Policy)

The authors equally contributed in the present research, at all stages from the formulation of the problem to the final findings and solution.

Sources of Funding for Research Presented in a Scientific Article or Scientific Article Itself

No funding was received for conducting this study.

Conflict of Interest

The authors have no conflicts of interest to declare.

APPENDIX

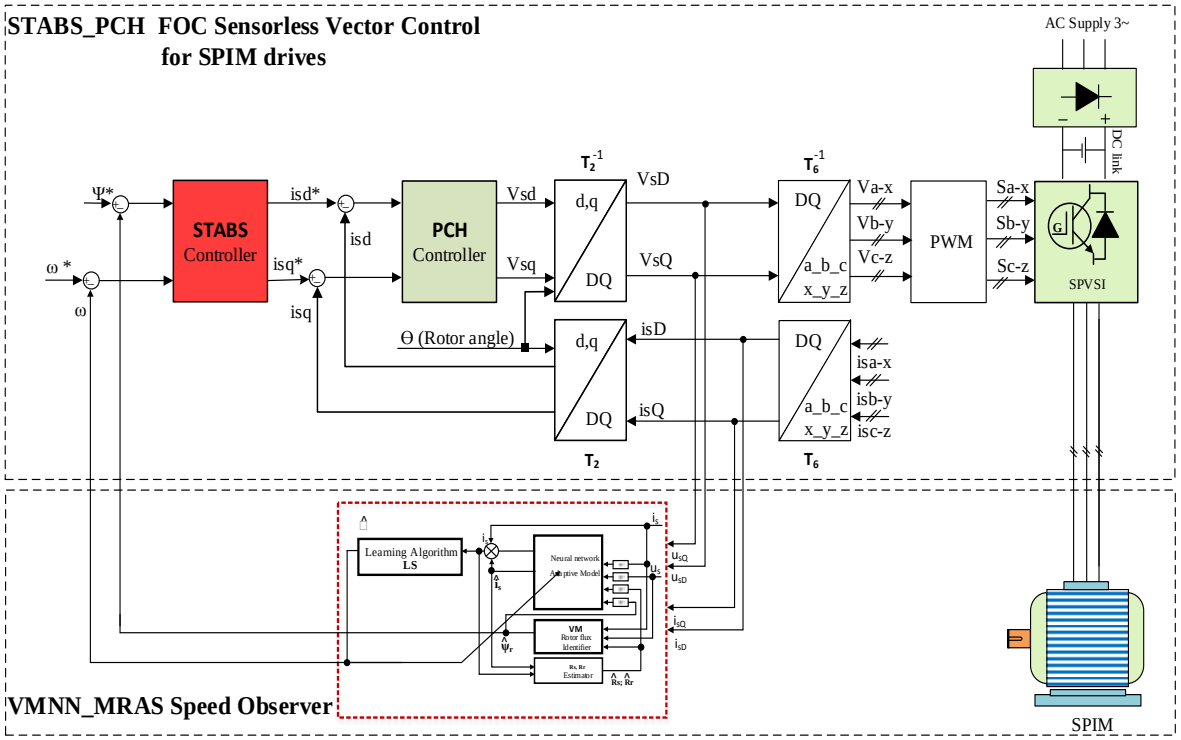

Fig. 4: Diagram of the proposed VM SC MRAS observer and STBS_PCH Control sensorless strategy

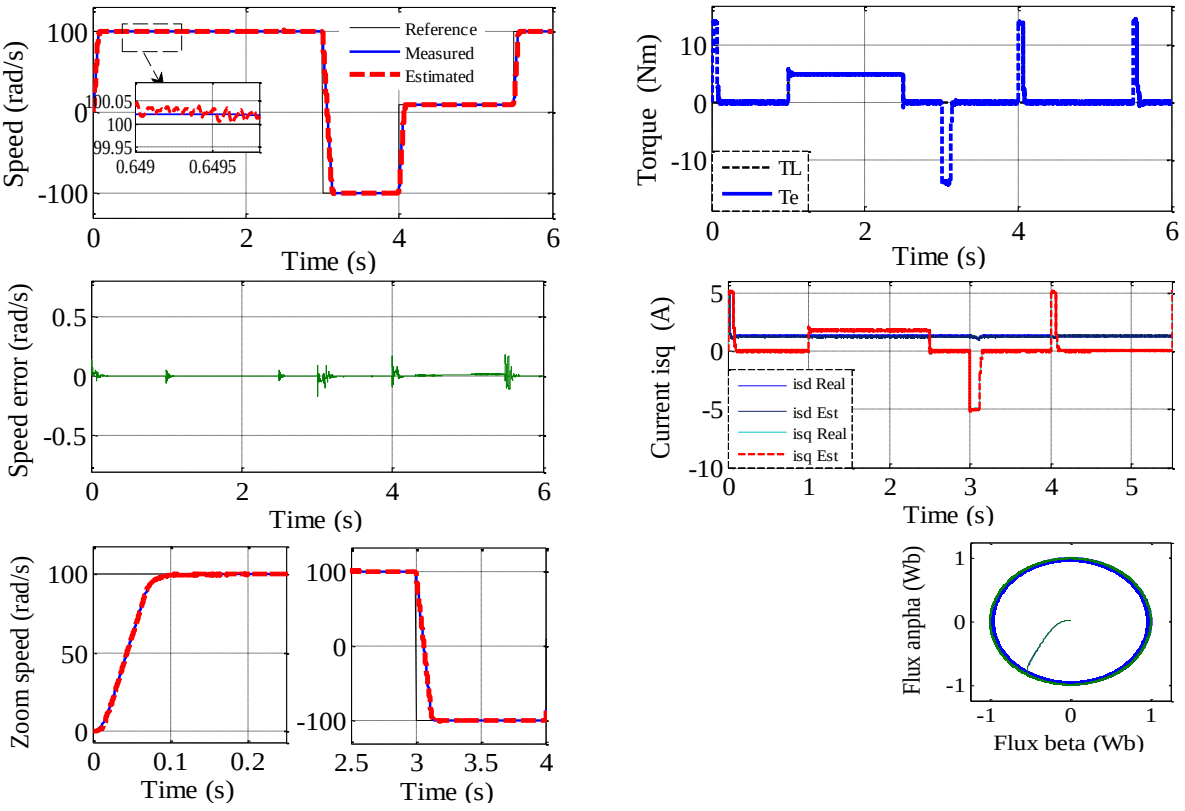

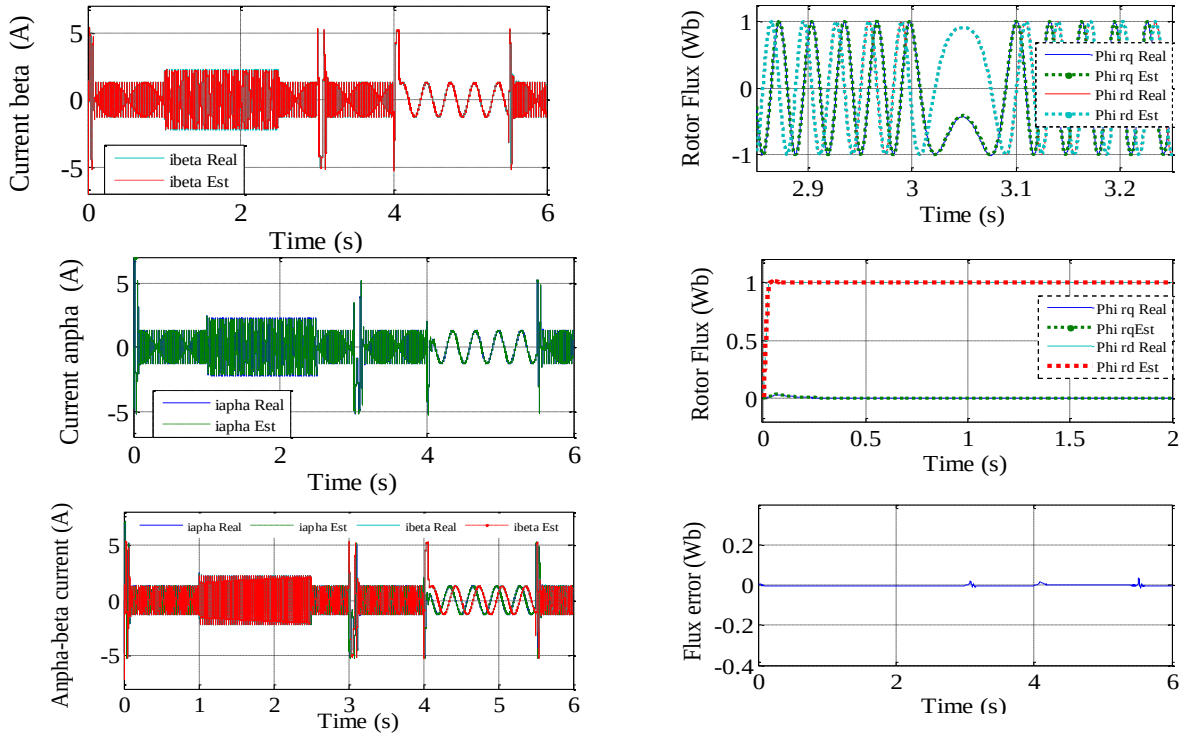

Fig. 5: The speed, torque, stator current, rotor flux responses, and estimated error in case of the speed and torque change of STABS_

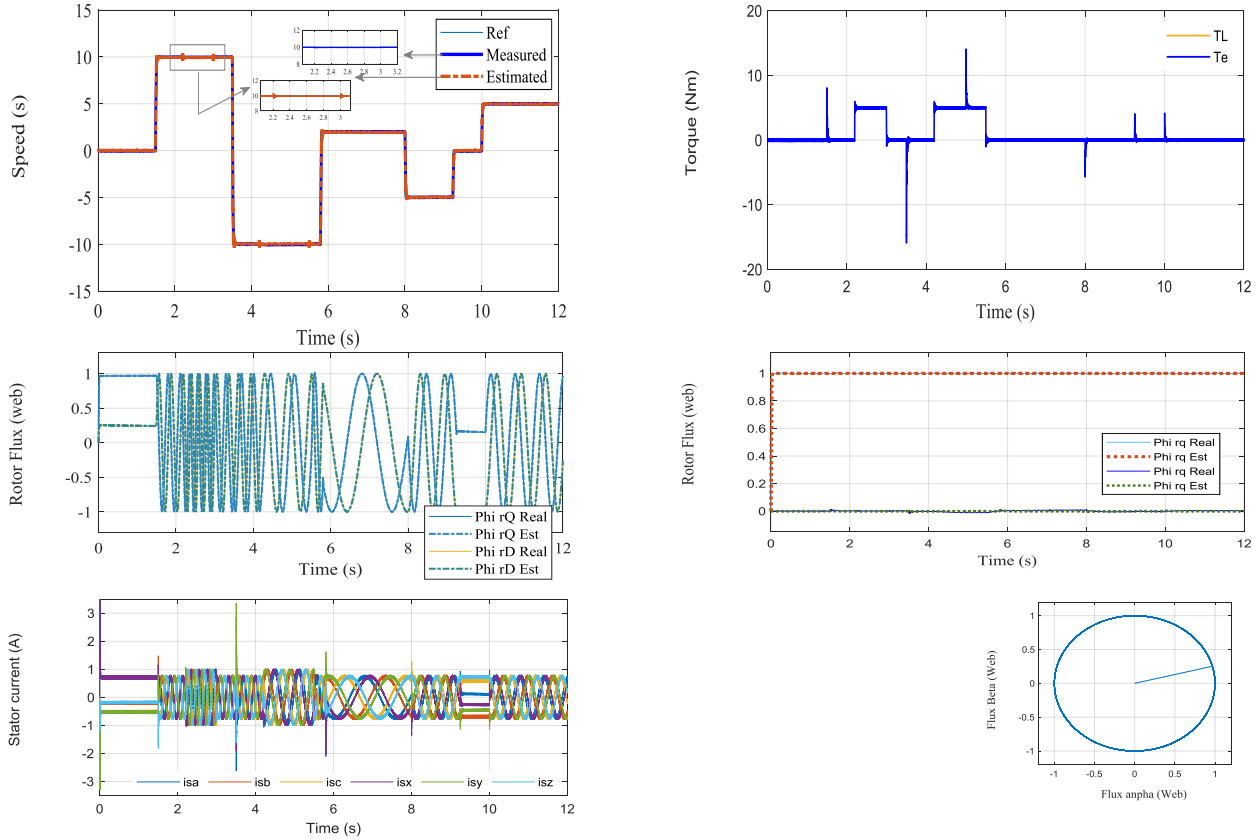

Fig. 7: Speed, Torque, Rotor Flux, and Stator current in case of the low speed both motor and regenerating modes